Supplement of Atmos. Meas. Tech., 18, 6933–6958, 2025 https://doi.org/10.5194/amt-18-6933-2025-supplement © Author(s) 2025. CC BY 4.0 License.





## Supplement of

# The Carbon Mapper emissions monitoring system

Riley Duren et al.

Correspondence to: Riley Duren (riley@carbonmapper.org)

The copyright of individual parts of the supplement might differ from the article licence.

## **Supplemental Information**

5

10

#### S1. Instrument design and performance

The Tanager instrument (Fig. S1) consists of a three-mirror anastigmat (TMA) telescope with a 22 cm aperture that focuses light at the slit of a Dyson spectrometer. The spectrometer consists of a lithographic slit, Dyson lens, grating, and focal plane array (FPA). The concentric Dyson spectrometer design offers higher optical throughput, with smaller footprint and lower mass than off-axis Offner spectrometers of similar performance (Mouroulis *et al.*, 2018). The spectrometer includes a CaF<sub>2</sub> glass Dyson lens and electron beam lithography-written diffraction grating on a concave, spherical substrate. The telescope mirrors are silver-coated and made from ultra-low expansion glass-ceramic material and are held strain-free via bipods attached to a carbon fiber composite optical bench assembly.

15 The telescope focuses light at the entrance slit of the spectrometer. In the spectrometer, the Dyson lens directs the light from the slit to the concave diffraction grating where the light is spectrally dispersed. From the grating, the first diffraction order light is directed back through the Dyson lens and focused onto the FPA after passing through an Order Sorting Filter (OSF), a three-zone bandpass filter that blocks unwanted grating orders. Straylight is minimized by the OSF, a zero-order light trap, and linear-variable anti-flection coating on the detector itself. 20 The FPA is a substrate-removed Mercury Cadmium Telluride detector array with 640x480 pixels and 30 µm pitch that defines the 5 nm spectral sampling. There are 640 pixels in the cross-track (spatial) dimension and 480 pixels in the spectral dimension. The FPA has a full well of about 1 million electrons to maximize SNR for darker images while avoiding saturation for brighter images and provides high quantum efficiency and linearity with low readout noise. A cryocooler maintains the FPA temperature at 160 K to minimize dark current. A precision 25 power supply unit and focal plane interface electronics minimize signal chain read noise in operating the FPA and providing analog to digital conversion. While the instrument can operate in a range of programmable integration times, the default value is ~8 ms (~ 125 frames per second). Digital instrument science data is sent to the spacecraft avionics for onboard storage and downlink.

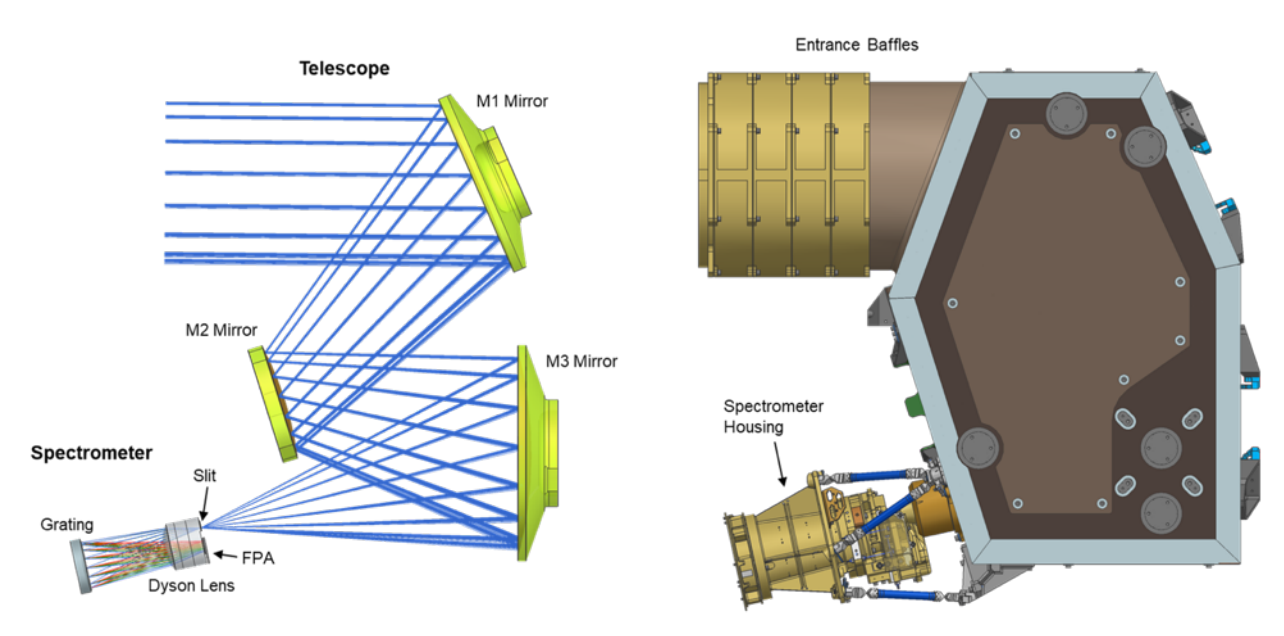


**Figure S1.** Tanager imaging spectrometer instrument. *Left*: Optical ray trace of telescope and the key Dyson spectrometer elements: slit, Dyson lens, grating, and Focal Plane Array (FPA). *Right*: the instrument optical bench assembly is composed of the entrance baffles, telescope housing, and Dyson spectrometer housing.

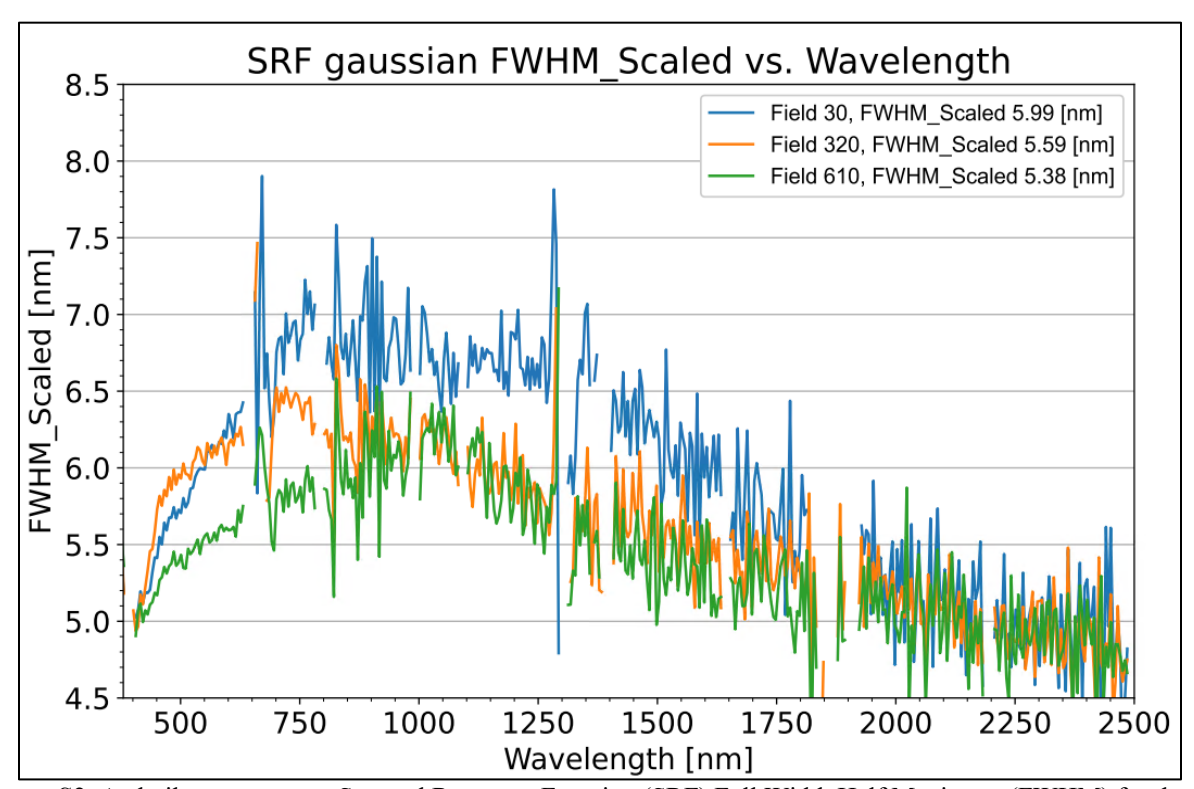


**Figure S2.** As-built spectrometer Spectral Response Function (SRF) Full Width Half Maximum (FWHM) for three columns spanning the cross-track direction based on lab testing with a monochromator. The average SRF approaches the spectral sampling of 5 nm in the critical SWIR bands for CH<sub>4</sub> and CO<sub>2</sub> retrievals (1960-2430 nm). For reference, the SRF for EMIT is approximately 8.5 nm FWHM.

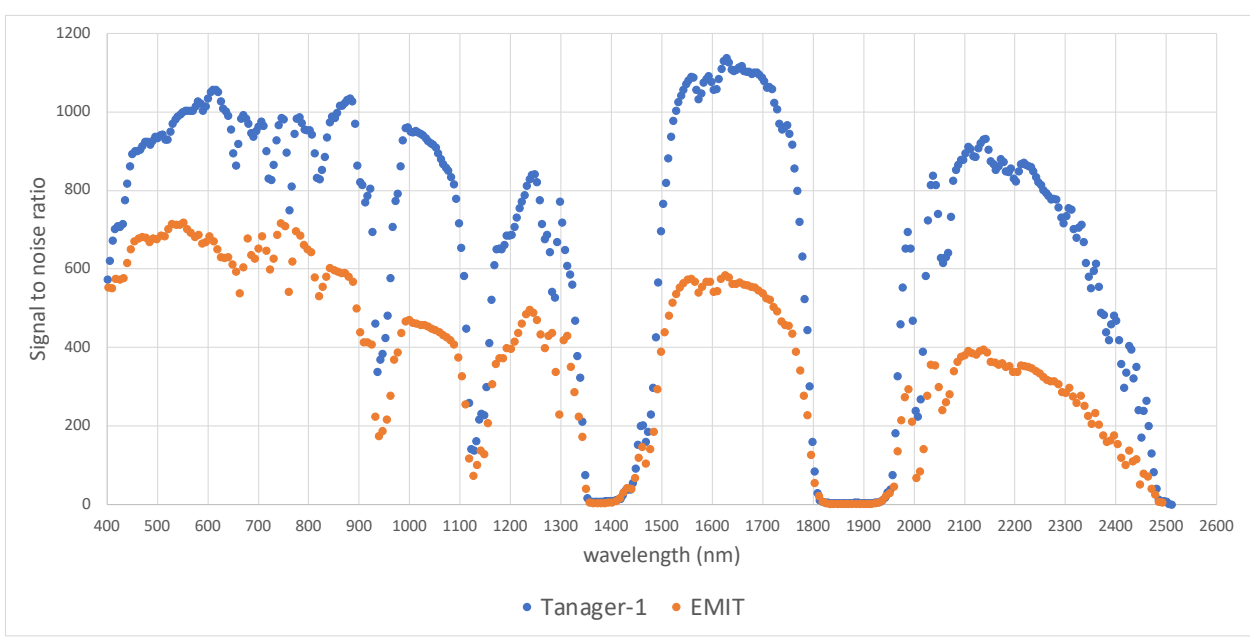


Figure S3. As-built spectrometer SNR across the full spectral range for Tanager-1 instrument compared with EMIT for reference. The Tanager values are for maximum sensitivity imaging mode (four stacked 8 millisecond exposures) and a 30 deg off-nadir viewing angle. EMIT is limited to nadir imaging (single 4 millisecond exposures). Both plots are for the same reference radiance with 35 deg solar zenith angle and 25% surface albedo.

Note the significantly higher Tanager SNR compared to EMIT in the key 2300 nm CH<sub>4</sub> retrieval band, enabled by Tanager's ground motion compensation capabilities.

#### S2. Planet Smallsat Platform

50

65

70

Planet's Smallsat Platform includes a common satellite bus used by both Planet's Pelican and Tanager (Carbon Mapper Coalition) constellations. The Smallsat Platform bus include a 600W power system, a high agility platform that can hold arc-second pointing accuracy and stability, multiple space qualified processors including state-of-the-art Field Programmable Gate Arrays (FPGAs), Graphics Processing Units (GPUs) and 2 Terabytes (TBs) of onboard storage capacity, low and high speed communication busses (CAN, Ethernet, SpaceFiber, PCIe), TT&C radio, high speed uplink and downlink radios, and advanced features such as real time intersatellite-link connectivity and an onboard Edge compute platform.

With a peak downlink rate of up to 10Gbps, each Tanager satellite is designed to be able to downlink at least 250 Gigabytes per day of hyperspectral data on average via a flexible global ground network. This data is backhauled from Planet's globally distributed ground stations to Planet's cloud platform for image processing, insight extraction, and dissemination including to Carbon Mapper's data platform. Four Ka-band ground stations are currently operational and actively supporting Tanager-1 and Planet's Pelican satellites. Table S1 summarizes the Tanager Smallsat Platform specifications.

**Table S1.** Tanager smallsat platform specifications

Parameter	Value
Orbit type	Sun Synchronous Orbit
Operational orbit altitude	406-430 km
Local Time of Descending Node	1100-1300 at the equator
Platform mass	200 kg (including 80 kg payload)
Design lifetime	5 years
Power (end of life)	600W generation, 650 Whr storage, 32V bus
Communications	S/X-band telemetry, tracking, command
	S-band high speed upre (512 kbps)
	Ka-band high speed downlink (10 Gbps)
Security	AER256 encryption on TT&C and imagery
	Link layer encryption on high speed downlink
Avionics/compute/storage	Space qualified processors, FPGAs, GPUs
	2 Terabytes onboard storage
Guidance, Navigation, Control	<10 arcsec pointing accuracy
	15 deg/sec slew rate
	Solar electric propulsion
	Dual band GPS receivers

#### S3. Level 1 data calibration and processing

Pre-launch calibration is conducted in a thermal-vacuum chamber to mimic on-orbit conditions, with optical subsystems (telescope, spectrometer, and detector) held at the midpoints of the allowable flight temperature performance ranges, within required thermal stability specifications (Zandbergen, *et al.* 2023). Each Tanager instrument undergoes the following pre-launch calibration testing program, including radiometric parameters measured with a National Institute of Standards and Technology (NIST) lamp and panel.

#### Spectral

- Spectral Range, Spectral Sampling, Spectral Calibration Knowledge
- Spectral Response (SRF)

85 Spatial

- Spatial Sampling Broadband Slit
- Cross-track Spatial Response Function (CRF)
- Along-track Spatial Response Function (ARF)
- Slit (Camera) Model

90

#### Uniformity

- Spectral Cross-track Uniformity (smile)
- Spectral IFOV Uniformity (keystone)
- 95 Radiometric
  - Radiometric Range (maximum reflectance)
  - Radiometric Calibration Uncertainty
  - Signal-to-Noise Ratio
  - Swath Width

100

### Stray Light

- In-field Spectral Scatter
- In-field Spatial Scatter
- Specular Ghosts

105

These in-lab measurements verify that the instruments meet the mission requirements and are used to generate initial calibration files. These files are an integral part of our data processing pipeline, allowing conversion of instrument Digital Numbers (DNs) to accurate physical units of radiance pre-launch.

- On-orbit, each Tanager regularly collects dark field calibration data, flat fields, and monitors for saturated pixels/bad pixels. Planet monitors each Tanager instrument Focal Plane Array's (FPA) drift in dark bias by frequent acquisition of "dark fields" throughout the satellite's life. Dark field collections are tasked automatically once per orbit. We use the Earth-facing acquisition strategy currently used by EMIT, imaging over regions specified in their existing dark ocean map. Multiple frames are acquired in a single dark field acquisition and are analyzed to identify and drop outliers, then aggregated to form a single dark bias estimate for use in subsequent image processing to correct the bias. Images are processed with their most recent dark field which are planned to meet Planet's quality standards.
- Additionally, the flat field can change on orbit across multiple spatial and temporal scales. Over short timescales, electronic drift in the amplifier and readout circuits can alter the sensitivity of distinct FPA elements and columns (e.g., due to temperature fluctuations or electromagnetic interference). Over longer periods, physical degradation or contamination of optical components can result in broader spatial changes. As a result, we monitor and update the laboratory flat field on orbit, both to support calibrated radiance data processing and to facilitate on-orbit instrument performance monitoring. As a baseline strategy, we collect flat fields over well-known calibration sites (i.e., PICS) on a monthly basis. These are acquired using standard collection modes as well as Side-Slither mode. Side-Slither mode enables the instrument to collect frames in a 90 degree rotation, making along-track movement aligned with cross-track elements. This determines that each element of the FPA covers the same area on the ground.
- The above process uses many of the scientific algorithms used in the NASA EMIT Science Data System, including the ISOFIT atmospheric correction algorithms (Thompson et al., 2018). These algorithms and associated code are openly available in GitHub and maintained by JPL.

During the 4 months following activation and checkout of the Tanager-1 spacecraft and instrument subsystems, a full scientific validation of instrument calibrations and calibrated radiance products was completed by Planet and JPL. Tanager satellites image a range of regularly used calibration/validation sites (e.g., RadCalNet, PICS), including those instrumented to collect coincident ground and atmospheric data. Initial calibration assessments based on in-lab measurements and adjustments (e.g., band wavelengths and radiometric calibration coefficients) have been made. The team also orchestrated a ground calibration campaign at Ivanpah Playa, California, in March 2025. Ground teams used field spectrometers to measure surface spectral reflectance and upward-looking sensors to measure surface solar irradiance and estimate atmospheric properties. Using procedures described by Bruegge *et al.*(2021), we can predict Tanager at-sensor radiance to validate and update the radiometric calibrations for the

satellite. A more comprehensive description of Tanager-1 spectrometer calibration will be published in a future paper.

## 145 S4. Retrieval, Plume Detection, Plume Segmentation, and Emission Rate Quantification Processing

#### Level 2 processing

For Tanager observations, the Carbon Mapper data platform uses calibrated radiance files delivered by Planet to derive several Level 2 data products. The L2 image outline products are the geographic boundaries, or "strips" of areas imaged by the Carbon Mapper Coalition satellites. Strip image outlines are helpful for determining where data is collected, the quality of that data, and verifying when methane or carbon dioxide sources are imaged, but no emissions above our detection limit were observed. In optimal observing conditions, such as an unobstructed view of the emission source and a high likelihood of detection, the absence of detection is termed a "null detect." The null detects imply that the source is not emitting methane above the sensor's minimum detection limit. We consider an image to be a good candidate for a null detect status for an emission source if the image contains less than 25% cloud cover and intersects any of the plume origin points estimated for the source. All Tanager L2 products are resampled to 30 meter resolution.

#### L2A Reference basemap images

L2A products are three-band (red-green-blue), natural color images of the Earth's surface generated from Tanager radiance files. This process involves correcting for atmospheric effects, geometric distortions, and terrain variations to produce accurate and visually appealing representations of the Earth. Carbon Mapper's operational workflow includes the use of Planet's Planetscope 5 meter resolution visible band images that are updated globally on a monthly cadence. In cases where Tanager's 30 meter spatial resolution is not sufficient to clearly identify the sector/facility type, Carbon Mapper may request high resolution (< 1 meter) visible band tasking from Planet's SkySat satellites. Carbon Mapper analysts use the various visible band image products and GIS data sets to help support attribution of observed CH<sub>4</sub> and CO<sub>2</sub> plumes to specific emission sectors, facilities, and, where possible, equipment types.

### L2B Atmospheric retrievals

L2B products consist of orthorectified full-strip atmospheric retrieval images derived by the Carbon Mapper data platform from L1B calibrated radiance files to retrieve column or concentration length CH<sub>4</sub> enhancements (units ppm-m) in the strong methane SWIR band between 2200-2400 nm and concentration length CO<sub>2</sub> enhancements between 1900-2100 nm.

#### 180 Column-wise Matched Filter

The column-wise matched filter (CMF) algorithm seeks an estimate for concentration length enhancement of CH<sub>4</sub> or CO<sub>2</sub> ( $\hat{\alpha}$ ) for each observed spectrum (Thompson et al., 2016; Thompson et al., 2015). This is done by testing each observed spectrum against a target signature ( $\vec{t}$ ), accounting for noise and background covariance  $\Sigma$ . At sensor radiance  $L_m$  (unit  $\mu$ W/cm/sr/nm) for a pixel affected by enhanced gas concentration is modeled through Beer-Lambert's Law:

$$L_m = L_o e^{-k\alpha}$$
 (1)

Where  $L_0$  represents at-sensor radiance in presence of background levels of a gas, and  $\vec{k}$  represents gas absorption. This model can be further simplified using Taylor expansion, assuming an optically thin plume:

$$L_m \approx L_o - \alpha t(L_o)$$
 (2)

185

Where  $t(L_0) = k * L_0$ , the unit absorption spectrum, as is calculated through radiative transfer simulations of transmittance. To estimate  $L_0$ , we use the mean spectrum  $\mu$  for all pixels in a "column" (i.e., all pixels in the flight direction of a single cross-track element) of observed data:

200

205

$$L_m \approx \mu - \alpha t(\mu)$$
 (3)

The optimal value of the concentration length,  $\hat{\alpha}$ , is found through optimization of log-likelihood - e.g., for the *i*th spectrum,  $\hat{\alpha}_i$  is the solution that minimizes the residual between observed and modeled spectra while accounting for covariance. The maximum likelihood solution takes the following form (Foote et al., 2021):

$$\hat{\alpha} = \frac{\mathbf{t}^T \, \mathbf{\Sigma}^{-1} (L_m - \, \boldsymbol{\mu})}{\mathbf{t}^T \, \mathbf{\Sigma}^{-1} \mathbf{t}} \tag{4}$$

The covariance matrix **Σ** is estimated from these same pixels in the along-track column. We employ a low-rank approximation for covariance to stabilize the solution in Equation 4, especially under regimes of few pixels per column (Thompson *et al.* 2015; Manolakis *et al.* 2009)

We follow the approach described in Foote et al., (2021) and select an image-specific unit absorption for each observation for both retrievals of CH<sub>4</sub> and CO<sub>2</sub> that depends on water vapor, ground elevation, and solar zenith angle. For column water vapor content, for each image acquisition, we query either the High Resolution Rapid Refresh (HRRR) meteorological product in the U.S. or the <u>European Centre for Medium-Range Weather Forecasts</u> <u>European Centre for Medium-Range Weather Forecasts</u> (ECMWF) Integrated Forecast System (IFS) meteorological product outside the U.S. For ground elevation, for the EMIT satellite instrument, we query values provided by that data source. For Tanager, we query the USGS GTOP030 Global Digital Elevation Map. For these dynamically queried or calculated parameters, we query a lookup-table database of unit absorption spectra that were precompiled and interpolated via MODTRAN simulations of various solar zenith angles, water vapor concentration, CH<sub>4</sub>/CO<sub>2</sub> background concentration, and surface heights (Foote *et al.* 2021).

### 225 Plume Detection

A point source is defined as the geographic location from which emissions originate that results in a highly concentrated plume of CH<sub>4</sub> or CO<sub>2</sub> gas in the atmosphere. Plumes are an excess mass of concentration in the atmosphere produced by a specific source. Plumes from point sources are a subset of a broader class of CH<sub>4</sub> or CO<sub>2</sub> enhancements that may occur anywhere in the atmosphere as a result of point source and/or diffuse area sources that may or may not be co-located with the enhancements (e.g., a "cloud" of enhanced CH<sub>4</sub> can appear in the atmosphere some distance downwind of the actual source). This is a critical concept: *not all observed atmospheric enhancements are the result of a point source emission nor can those enhancements be reliably attributed to a specific emission source*. Therefore, Carbon Mapper point source detection and quality control procedures require that any detected atmospheric plume must be related to a credible point source on the earth's surface before reporting. Any observed enhancements that fail to meet QC checks are noted for potential follow-up study but do not result in published plumes or emission rate estimates.

The Carbon Mapper point source detection process relies on concentration retrievals (CH<sub>4</sub> and CO<sub>2</sub> band images), visible red-green-blue (RGB) imagery from various observing systems, GIS data sets, and meteorological data. The process begins with automated application of CH<sub>4</sub> and CO<sub>2</sub> retrieval algorithms to every calibrated radiance strip image generated by a satellite or airborne sensor. This results in grayscale CH<sub>4</sub> and CO<sub>2</sub> band images that first undergo strip image level QC review by human analysts. This review includes determination of systematic issues affecting the entire strip image, including retrieval processing problems, atmospheric artifacts (high haze, clouds, smoke, etc), geolocation issues, or excessive noise. Each image's CH<sub>4</sub> and CO<sub>2</sub> band images are then reviewed to detect potential point source plumes along with geolocation of their likely origins.

Level 3-4 processing

#### **Plume Segmentation**

250

230

235

240

Following detection, Carbon Mapper implements an automated plume segmentation and delineation process on identified and geolocated plumes. This process separates the background from enhanced CH<sub>4</sub>/CO<sub>2</sub> pixels to create a masked plume boundary that is used for mass and emission quantification. The segmentation algorithm proceeds as follows:

255

260

- 1. The L2B concentration map is cropped around the origin of a plume: ±2500 meters in both directions
- 2. A concentration threshold is dynamically determined to separate lingering background enhancements from plume enhancements. This threshold is subtracted off the cropped concentration map around the plume origin.
- 3. Connected pixels of enhanced concentration (> ppm-m threshold) are grouped together. A cluster must contain 5 pixels to be considered part of the plume.
- 4. A proximity metric is enforced on each cluster group. Separated clusters that exceed 15 pixels from the plume origin are excluded from the plume

265

#### **Plume Emission Quantification**

For emissions quantification, we apply the Integrated Mass Enhancement (IME) approach, which calculates the excess mass in units of kilograms emitted to the atmosphere from a source (Thompson *et al.* 2016):

270

$$IME = \alpha \sum_{i=1}^{P} \Omega_i A_i \quad (5)$$

Where *i* refers to a single plume pixel, *P* is the number of pixels in the segmented plume mask,  $\Omega$  is the concentration enhancement of that pixel,  $\alpha$  is a unit conversion scalar (from ppm-m to kg/m<sup>2</sup>), and A is the area of that pixel (m<sup>2</sup>). We calculate an emission rate Q using the following relationship (Duren *et al.* 2019):

275

280

285

$$Q = \frac{IME}{L}U \quad (6)$$

Where U is the 10-m wind speed (m/s) and L is the plume length (m). Here U is taken from the HRRR 3km, 60 minute reanalysis product for observations within the U.S. and the ECMWFIFS 9 km product outside the U.S. Forecast versions of these products may be used for initial quick-look processing given standard latencies in receiving reanalysis products. In Equation 6, L is estimated as the maximum distance along the segmented plume's convex hull. For plumes covering large spatial distances, we impose a distance constraint such that the segmented plume mask is clipped to not exceed a 2500 m radial extent from the origin of the plume. Therefore, L= min{max(hulldist), 2500m}. The IME (Equation 5) is also only calculated within this clipped plume mask. This clipping procedure is employed to reduce bias that may affect IME quantification due to differing surface and meteorological conditions across large plumes, intermittency of the emission rate of the source, and to limit potential merging of multiple plumes downwind of their sources.

Uncertainties in emission estimates are calculated by summing in quadrature elements that contribute to variability in emissions:

$$\sigma_{q} = \sqrt{\left(\frac{\partial Q}{\partial U}\sigma_{U}\right)^{2} + \left(\frac{\partial Q}{\partial IME}\sigma_{IME}\right)^{2} + \left(\frac{\partial Q}{\partial L}\sigma_{L}\right)^{2}}$$
(7)

Where

295

300

$$\sigma_{IME} = \frac{\partial Q}{\partial IME} \sigma_N + \frac{\partial Q}{\partial \Omega} \sigma_\Omega$$
 (8)

In Equation 7 - the  $(\frac{\partial Q}{\partial U}\sigma_U)$  term represents the uncertainty due to wind speed, which we estimate by computing the standard deviation of 10-m wind estimates across the hour before and after the plume detection. The  $(\frac{\partial Q}{\partial IME}\sigma_{IME})$  term is decomposed into two components, first uncertainty due to masking, which we parameterize as the standard deviation of IME estimates across a range of segmented plume masks, and second uncertainty due to the retrieval, which was estimate as the standard deviation of concentration enhancements outside of the segmented plume mask,

but within a 2500 m crop of the plume. Finally, the  $(\frac{\partial Q}{\partial L}\sigma_L)$  represents an irreducible uncertainty term due to the pixel resolution of the satellite instrument and how it affects the estimate of plume length L. Figure S4 shows the effect of this term: the edge of a plume may manifest as concentration enhancement in a single or multiple pixels depending on the true geolocation of the plume and the spatial resolution of the instrument.

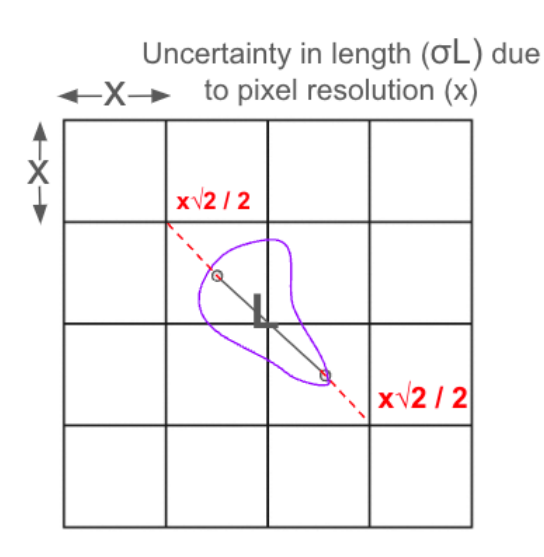


Figure S4. Irreducible uncertainty due to pixel resolution for IME quantification approaches.

#### **Quick look products**

305

310

315

320

325

Carbon Mapper's workflow generates quick-look data products with a mean latency of < 36 hours following each observation. The quick-look product generation process includes a round of initial QC review by human analysts that generates quality flags for each plume that includes but are not limited to:

#### Strip image-level quality attributes

- Image artifacts [column, glint, flare, contrast, other]
- Low signal-to-noise flag
- Atmospheric artifacts [clouds, smoke, haze, other]
- Cloud cover fraction [0, 25, 50, 75, 100] or [0-1]

#### Plume-level quality attributes

- Overall rating (Good, Questionable, or Bad)
- plume shape flag
- artifacts intersect plume flag
- flare flag
- high background enhancement flag

#### **Final Processing and Publication**

Following generation of quick-look products, Level 4 processing proceeds with additional QC review of the initial emission estimate and additional processing including the use of reanalysis products in place of forecast wind fields. In some cases where there is high confidence in a plume detection but there are concerns with the fidelity of the emission estimate, Carbon Mapper will publish the plume image and coordinates but without an emission estimate. In addition to delivering final version of plume-level images, emission estimates, uncertainties and sector attribution, Level 4 processing includes aggregating a time-series of plumes to a specific emission source on the earth's surface and calculating persistence-adjusted average emission rates for that source following methods described in Cusworth et al., 2021a. The resulting plume raster images and tabular information on emission rates, plume/source coordinates, sector attribution, detection dates/times, source persistences, and associated uncertainties as well as our Level 2 strip-

image level products are published via Carbon Mapper's public data portal and available for API and bulk download 30 days following each Tanager observation. Additional Carbon Mapper documentation including our Data Product Guide, Algorithm Theoretical Basis Documents, and Quality Control Description Document are available in the Technical Resources section of our website (<a href="https://carbonmapper.org/resources/technical-resources">https://carbonmapper.org/resources/technical-resources</a>).

## 345 S5. Controlled Release Testing Setup

350

355

360

Natural gas was released from a system consisting of a compressed natural gas trailer connected to a pressure regulation trailer and a gas metering trailer. Flow rates were metered using one of three parallel-mounted Emerson Micromotion Coriolis flow meters, directing gas through a 7.3 m stack controlled by a butterfly valve (El Abbadi *et al.*, 2024). The flow rate was controlled virtually via a flow control system on the metering trailer. Meteorological data were collected near the release point at 10 m (Campbell Scientific CAST3B, 3D) and 2 m (Campbell Scientific METSENS500, 2D) heights, providing measurements of wind speed and wind direction at 10 m and 2 m as well as relative humidity, dew point, temperature, and atmospheric pressure at 2 m. The test team also tracked natural gas composition, which ranged from 92.7% to 94.5% CH4 throughout the unblinded period. In Evanston, six unblinded releases were conducted, with emission rates ranging from 186.1 (± 3.5% 95% CI) to 694.2 (±3.59% 95% CI) kg/h. In Casa Grande, nine releases ranged from 98.85 (± 8.57% 95% CI) to 951.5 (± 5.34% 95% CI) kg/h. During the unblinded period, mean wind speeds in Evanston were 4.78 m/s within 30 minutes of noon and mean wind speeds in Casa Grande were 2.16 m/s within 30 minutes of noon. Release rates and meteorological observations were rapidly shared following Tanager satellite overpasses during this period, and can be found in this repository: <a href="https://doi.org/10.25740/qh001qt3946">https://doi.org/10.25740/qh001qt3946</a> (Reuland et al., 2025). The releases during this unblinded period were performed cooperatively, with flow rates and durations suggested by the Carbon Mapper team.

Uncertainties associated with this controlled release configuration are smaller than those associated with the quantification of gas flow rates from satellites. The accuracy of the metered gas flow rate as metered by Emerson Micromotion Coriolis flow meters ranged from ± 0.25% for the large (CMFS150M) and small (CMFS015H) meters, to ± 0.35% for the medium meter (CMF050M). Uncertainties associated with the meteorological measurements were also small. 10-m measurements from the CSAT3B has a maximum offset error in wind speed of ±8 cm/s (U<sub>x</sub>, U<sub>y</sub>) and ± 4 cm/s (U<sub>z</sub>), and a maximum gain error of ±2%, 3%, or 6% depending on whether wind vector is within 5, 10, or 20 degrees of horizontal respectively. The 2-m measurements from the METSENS500 were accurate in wind speed to within 3% and wind direction to within 5 degrees up to 40 m/s, with those figures changing to 5% and 5 degrees for winds between 40 m/s and 60 m/s.

## 375 <u>SI6. Geographical Distribution of Plume Detections</u>

As of August 15, 2025, about 5600 CH<sub>4</sub> and about 1200 CO<sub>2</sub> point source emission plumes have been detected in Tanager-1 scenes, 85% were detected following the end of commissioning on January 31, 2025. See Fig. S5.

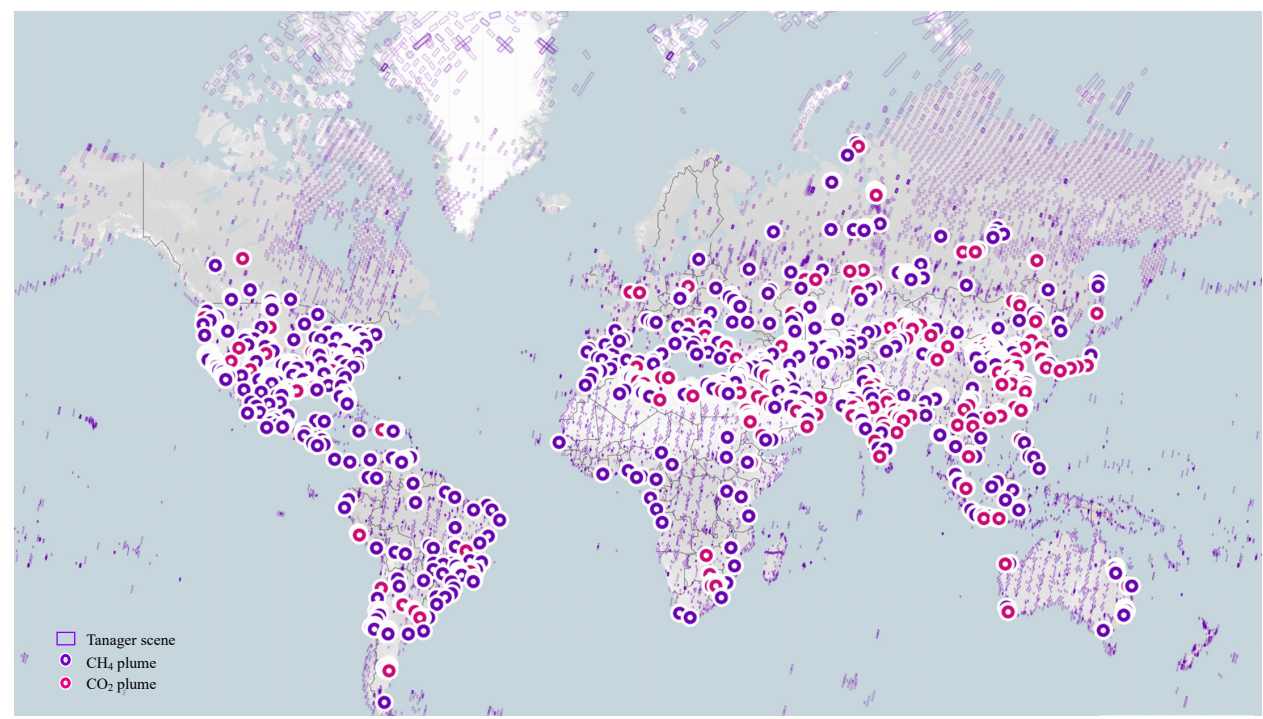


Figure S5. Geographic distribution of CH<sub>4</sub> and CO<sub>2</sub> plumes detected in Tanager-1 scenes between September 16, 2024 and August 15, 2025.

#### 385 References

380

390

405

Bruegge, C.J., Arnold, G.T., Czapla-Myers, J., Dominguez, R., Helmlinger, M.C., Thompson, D.R., Van den Bosch, J. and Wenny, B.N. Vicarious calibration of eMAS, AirMSPI, and AVIRIS sensors during FIREX-AQ. *IEEE Transactions on Geoscience and Remote Sensing*, *59*(12), 2021.

Duren, R.M., Thorpe, A.K., Foster, K.T., Rafiq, T., Hopkins, F.M., et al. "California's Methane Super emitters." *Nature* 575 (7781): 180–84. https://doi.org/10.1038/s41586-019-1720-3, 2019.

Foote, M.D., Dennison, P.E., Thorpe, A.K., Thompson, D.R., Jongaramrungruang, S., Frankenberg, C., and Joshi, S.C., "Fast and Accurate Retrieval of Methane Concentration From Imaging Spectrometer Data Using Sparsity Prior." *IEEE Transactions on Geoscience and Remote Sensing* 58 (9): 6480–92. https://doi.org/10.1109/TGRS.2020.2976888, 2021.

Manolakis, D. et al. "Hyperspectral detection algorithms: use covariances or subspaces?." Imaging Spectrometry
XIV. Ed. Sylvia S. Shen & Paul E. Lewis. San Diego, CA, USA: SPIE, 2009. 74570Q-8,
http://dx.doi.org/10.1117/12.828397

Mouroulis, P., Robert O. Green, "Review of high fidelity imaging spectrometer design for remote sensing," *Opt. Eng.* 57(4), 040901, doi: 10.1117/1.OE.57.4.040901, 2018

Reuland, F., Adams, T., Kort, E. A., and Brandt, A. R. (2025). Large-Scale Controlled Methane Releases for Satellite-Based Detection and Emission Quantification of Methane Point-Sources. Version 5. Stanford Digital Repository. Available at https://purl.stanford.edu/qh001qt3946/version/5. https://doi.org/10.25740/qh001qt3946.

Thompson, D. R., I. Leifer, H. Bovensmann, M. Eastwood, M. Fladeland, C. Frankenberg, K. Gerilowski, et al. "Real-Time Remote Detection and Measurement for Airborne Imaging Spectroscopy: A Case Study with Methane." Atmospheric Measurement Techniques 8 (10): 4383–97. https://doi.org/10.5194/amt-8-4383-2015, 2015.

- Thompson, D. R., Thorpe, A. K., Frankenberg, C., Green, R. O., Duren, R., Guanter, L., Ungar, S.. Space-based remote imaging spectroscopy of the Aliso Canyon CH4 superemitter. *Geophysical Research Letters*, 43(12), 2016.
- Thompson, D. R., V. Natraj, R. O. Green, M. C. Helmlinger, B-C Gao, and M. L. Eastwood. "Optimal estimation for imaging spectrometer atmospheric correction." *Remote sensing of environment* 216, 2018.

415

Zandbergen, S.R., Shaw, L., Klein, C., Thompson, D.R., Green, R.O., Duren, R., Gibson, M., Nazaryan, H., Smith, C., Cubanski, B., Giuliano, P., Haag, J.M., and Pritchett, C., "Preliminary alignment, characterization, and comparison of next generation carbon mapping imaging spectrometers", *Proc. SPIE 12688, Imaging Spectrometry XXVI: Applications, Sensors, and Processing, 126880C* (30 October 2023); https://doi.org/10.1117/12.2678614, 2023.